universe

IMPACT FACTOR 2.813

CITESCORE 3.2

Article

DE Models with Combined $H_0 \cdot r_d$ from BAO and CMB Dataset and Friends

Denitsa Staicova

Special Issue

Modified Gravity Approaches to the Tensions of ΛCDM

Edited by

Dr. Eleonora Di Valentino, Prof. Dr. Leandros Perivolaropoulos and Dr. Jackson Levi Said

MDPI

https://doi.org/10.3390/universe8120631

universe

MDPI

Article

DE Models with Combined $H_0 \cdot r_d$ from BAO and CMB Dataset and Friends

Denitsa Staicova

Institute for Nuclear Research and Nuclear Energy, Bulgarian Academy of Sciences, 1784 Sofia, Bulgaria; dstaicova@inrne.bas.bg

Abstract: It has been theorized that dynamical dark energy (DDE) could be a possible solution to Hubble tension. To avoid degeneracy between Hubble parameter H_0 and sound horizon scale r_d, in this article, we use their multiplication as one parameter $c/(H_0 r_d)$, and we use it to infer cosmological parameters for 6 models—ΛCDM and 5 DDE parametrizations—the Chevallier–Polarski–Linder (CPL), the Barboza–Alcaniz (BA), the low correlation (LC), the Jassal–Bagla–Padmanabhan (JBP) and the Feng–Shen–Li-Li models. We choose a dataset that treats this combination as one parameter, which includes the baryon acoustic oscillation (BAO) data $0.11 \leq z \leq 2.40$ and additional points from the cosmic microwave background (CMB) peaks ($z \simeq 1090$). To them, we add the marginalized Pantheon dataset and GRB dataset. We see that the tension is moved from H_0 and r_d to $c/(H_0 r_d)$ and Ω_m. There is only one model that satisfies the Planck 2018 constraints on both parameters, and this is LC with a huge error. The rest cannot fit into both constraints. ΛCDM is preferred, with respect to the statistical measures.

Keywords: cosmological tensions; dynamical dark energy; baryon acoustic oscillation; Pantheon dataset; gamma-ray bursts

Citation: Staicova, D. DE Models with Combined $H_0 \cdot r_d$ from BAO and CMB Dataset and Friends. *Universe* **2022**, *8*, 631. https://doi.org/10.3390/universe8120631

Academic Editor: Antonino Del Popolo

Received: 1 November 2022
Accepted: 24 November 2022
Published: 28 November 2022

1. Introduction

The quest for understanding cosmological tensions has driven research for years now. It seems that the tension between the direct measurements of the Hubble constant (H_0) from the late universe ([1–5]) and that from the early universe (i.e., from measuring the temperature and polarization anisotropies in the cosmic microwave background [6–9]) is only aggravated with the increase in the precision and knowledge of the systematics of the data and has reached 5 σ. This discrepancy has spurred many works, trying to resolve whether the dark energy is a constant energy density or with a dynamical behavior, and if so, of what origin, leading to many different theories and possible explanations [10–21].

There are many dark energy (DE) parametrizations [22–25] that can be used in the search for deviations from the cosmological constant, Λ. Some of them fall in the group of early dark energy models [26–30], which modify physics of the early universe. Others modify the late-time universe physics, such as in the phantom dark energy [31,32] models, and emergent dark energy [33,34], add interaction in the DE sector, as in the interacting dark energy [35–37], or add exotic species or scalar fields [38–42]. For a review on the taxonomy of DE models, see Refs. [43–45]. Finally, there is the generalized emergent dark energy (GEDE) [45] found to be able to compete with ΛCDM for some BAO datasets [46]. In this work, we take the so-called dynamical dark energy parametrizations, which allow for a non-constant DE contribution, regardless of the origin behind it. We take a number of models, namely the Chevallier–Polarski–Linder (CPL), the Barboza–Alcaniz (BA), the low correlation (LC), the Jassal–Bagla–Padmanabhan (JBP) and the Feng–Shen–Li–Li (FSLLI) model, and we use statistical measures to judge their performance in fitting the data.

An important part of the tensions debate revolves around the role of the sound horizon at drag epoch r_d. At recombination, after the onset of CMB at $z_* \simeq 1090$, the baryons escape

the drag of photons at the drag epoch, $z_d \simeq 1059$ (Planck 2018 [7]). This sets the standard ruler for the baryon acoustic oscillations (BAO)—the distance (r_d) at which the baryon–photon plasma waves oscillating in the hot universe froze at $z = z_d$. The sound horizon at drag epoch is given by

$$r_d = \int_{z_d}^{\infty} \frac{c_s(z)}{H(z)} dz, \tag{1}$$

where $c_s \approx c(3 + 9\rho_b/(4\rho_\gamma))^{-0.5}$ is the speed of sound in the baryon–photon fluid with the baryon $\rho_b(z)$ and the photon $\rho_\gamma(z)$ densities, respectively [47,48].

Many papers discuss the relation between the H_0 and the sound horizon scale r_d for different models [49–51]. Any DE model claiming to resolve the H_0 tension should also be able to resolve the r_d tension since they are strongly connected [51–53]. In other words, setting a prior on r_d has a very strong effect on H_0 and vice versa. In this paper, to avoid this problem, we combine the H_0 and r_d into one parameter. We choose measurements that combine the H_0 and r_d from the BAO and the prior distance from the CMB peaks [54–62] and we use them to infer the cosmological parameters for ΛCDM and 5 DDE models. To the BAO+CMB dataset, we add the gamma-ray bursts (GRB) dataset and the Pantheon dataset with similarly marginalized dependence on H_0 (and M_B). We do this to expand the redshift considered by the models. In a previous work [46], we used a similar approach in which we integrated $H_0 r_d$ in the χ^2 of the model, while here, we use them as one single quantity without modifying the χ^2. In the marginalized version, we saw an interesting possibility for some DE model to fit the data better than ΛCDM. We continue this investigation with new models and a new approach in this paper.

Historically, the approach of using the combination $H_0 r_d$ is not new. It has been used in [63] with BAO and SN data to find consistency with the Planck 2015 best-fit ΛCDM cosmology; Ref. [64] used the BAO data to fit the growth measurement, again finding consistency with the Planck 2015; Ref. [65] used the Cepheids and the Tip of the Red Branch measurements to calibrate BAO and SN measurements and find significant tension in both H_0 and r_d, despite testing the ΛCDM and DE models (EDE, $wCDM$, pEDE). The implication is that modifications of the physics after recombination fail to solve both tensions. The overall conclusion is that the H_0 tension should not be considered separately from the r_d measurement implied by it [66]. In the current work, we choose a different approach. We repeat the analysis on $H_0 r_d$ used in earlier works, but we also take the ratio r_*/r_d as an independent parameter. This means that we do not use the known analytical formulas for them, but instead we use MCMC to infer them. This avoids using explicit prior knowledge on the baryon load of the universe. This way, we avoid both the degeneracy on $H_0 r_d$ from the BAO data, but also we do not use as a hidden prior the Planck measurements.

The plan of the work is as follows: Section 2 formulates the relevant theory. Section 3 describes the method. Section 5 shows the results, and Section 6 summarizes the results.

2. Theory

A Friedmann–Lemaître–Robertson–Walker metric with the scale parameter $a = 1/(1+z)$ is considered, where z is the redshift. The evolution of the universe for it is governed by the Friedmann equation, which connects the equation of the state for the ΛCDM background:

$$E(z)^2 = \Omega_r(1+z)^4 + \Omega_m(1+z)^3 + \Omega_k(1+z)^2 + \Omega_{DE}(z), \tag{2}$$

where in standard ΛCDM, $\Omega_{DE}(z) \rightarrow \Omega_\Lambda$, with the expansion of the universe $E(z) = H(z)/H_0$, where $H(z) := \dot{a}/a$ is the Hubble parameter at redshift z, and H_0 is the Hubble parameter today. Ω_r, Ω_m, Ω_{DE} and Ω_k are the fractional densities of radiation, matter, dark energy and the spatial curvature at redshift $z = 0$. We take into account the radiation energy density as $\Omega_r = 1 - \Omega_m - \Omega_\Lambda - \Omega_k$. The spatial curvature is expected to be zero for a flat universe, $\Omega_k = 0$, and we set it to zero because we focus on DE models.

We will consider a number of different DE models, all of which will feature a dark energy component depending on z. This can be done with a generalization of the Chevallier–Polarski–Linder (CPL) parametrization [67–69]:

$$\Omega_{DE}(z) = \Omega_\Lambda \exp\left[\int_0^z \frac{3(1+w(z'))dz'}{1+z'}\right] \tag{3}$$

which allows for three possible models from which we will consider only the CPL:

$$w(z) = w_0 + w_a \frac{z}{z+1} \tag{4}$$

and ΛCDM is recovered for $w_0 = -1, w_a = 0$.

To this parametrization, we add another model [43,70], which is the Barboza–Alcaniz (BA) model with

$$w(z) = w_0 + z\frac{1+z}{1+z^2}w_1 \tag{5}$$

This model is good for describing the whole universe history because it does not diverge for $z \to -1$. It gives

$$\Omega_{DE} = \Omega_\Lambda (1+z)^{3(1+w_0)}(1+z^2)^{\frac{3w_1}{2}}. \tag{6}$$

Next, we use the low correlation model (LC) [43,71] with

$$w(z) = \frac{(-z+z_c)w_0 + z(1+z_c)w_c}{(1+z)z_c} \tag{7}$$

where $w_0 = w(0)$ and $w_c = w(z_c)$ where z_c is the redshift at which w_0 and w_z are uncorrelated. The effective entry into the EOS is

$$\Omega_{DE} = \Omega_\Lambda (1+z)^{(3(1-2w_0+3wa))} e^{\frac{9(w_0-wa)z}{(1+z))}} \tag{8}$$

where, here, are replaced w_c with w_a for consistency with the other models.

The Jassal–Bagla–Padmanabhan (JBP) parametrization [44,72]

$$w(z) = w_0 + w_1 \frac{z}{(1+z)^2} \tag{9}$$

which gives

$$\Omega_{DE} = \Omega_\Lambda (1+z)^{3(1+w_0)} e^{\frac{3w_1 z^2}{2(1+z)^2}} \tag{10}$$

with $w_0 = w(z=0)$ and $w_1 = (dw/dz)_{|(z=0)}$.

Finally, we will also test the Feng–Shen–Li–Li parametrization [44,73] which is divergence-free for the entire history of the universe. It has two cases:

$$w(z)^+ = w_0 + w_1 \frac{z}{1+z^2} \tag{11}$$

$$w(z)^- = w_0 + w_1 \frac{z^2}{1+z^2} \tag{12}$$

with the final contribution to the EOS of each of them being, accordingly,

$$\Omega_{DE}^\pm = \Omega_\Lambda (1+z)^{3(1+w_0)} e^{\pm\frac{3w_1}{2}\arctan(z)} (1+z^2)^{\frac{3w_1}{4}} (1+z)^{\mp\frac{3}{2}w_1} \tag{13}$$

In this work, the plus case (i.e., Ω_{DE}^+) is denoted as FSLLI, and the minus case (i.e., Ω_{DE}^-) is denoted as FSLLII.

The distance priors provide effective information of the CMB power spectrum in two aspects: the acoustic scale $l_{\rm A}$ characterizes the CMB temperature power spectrum in the transverse direction, leading to the variation of the peak spacing, and the "shift parameter" R influences the CMB temperature spectrum along the line-of-sight direction, affecting the heights of the peaks. The popular definitions of the distance priors are [74]

$$\begin{aligned} l_{\rm A} &= (1+z_*)\frac{\pi D_{\rm A}(z_*)}{r_s(z_*)}, \\ R &\equiv (1+z_*)\frac{D_{\rm A}(z_*)\sqrt{\Omega_m}H_0}{c}, \end{aligned} \tag{14}$$

where z_* is the redshift at the photon decoupling epoch with $z_* \simeq 1089$ according to the Planck 2018 results [7]. r_* is the co-moving sound horizon at $z = z_*$. Ref. [57] derives the distance priors in several different models using Planck 2018 TT,TE,EE + lowE which is the latest CMB data from the final full-mission Planck measurement [7]. We use the correlation matrices given in Table 1 in [57] to obtain the covariance matrices for l_A and R corresponding to each model.

The angular diameter distance, $D_{\rm A}$, needed for both the distance priors and the BAO points, is given by

$$D_{\rm A} = \frac{c}{(1+z)H_0\sqrt{|\Omega_k|}}\text{sinn}\left[|\Omega_k|^{1/2}\int_0^z \frac{dz'}{E(z')}\right], \tag{15}$$

where $\text{sinn}(x) \equiv \sin(x), x, \sinh(x)$ for $\Omega_k < 0$, $\Omega_k = 0$, $\Omega_k > 0$, respectively. We see that for the measured D_A/r_d, one can isolate the variable $b = c/(H_0 r_d)$. Below, we set $\Omega_k = 0$, so this formula simplifies to

$$\frac{D_{\rm A}}{r_d} = \frac{b}{(1+z)}\int_0^z \frac{dz'}{E(z')} \tag{16}$$

Finally, for the SN and GRB datasets, we define the distance modulus $\mu(z)$, which is related to the luminosity distance ($d_L = D_A(1+z)^2$), through

$$\mu_B(z) - M_B = 5\log_{10}[d_L(z)] + 25\,, \tag{17}$$

where d_L is measured in units of Mpc, and M_B is the absolute magnitude.

3. Methods

In this paper, we use three datasets, which we treat differently. For the BAO dataset, the definition of χ^2, which we minimize, is the standard one since we do not use the covariance matrix for it.

$$\chi^2_{BAO} = \sum_i \frac{(\vec{v}_{obs} - \vec{v}_{model})^2}{\sigma^2}, \tag{18}$$

where $\vec{v}_{obs}$ is a vector of the observed points (i.e., the values of D_A/r_d at each z in Table A1), $\vec{v}_{model}$ is the theoretical prediction of the model calculated with Equation (16) and σ is the error of each measurement.

Additionally, we use the SN and the GRB datasets to further constrain the models. For them, we use the following marginalized over H_0 and M_B formula, taken from [46] so that we avoid setting priors on H_0 and M_B.

Following the approach used in ([75–78]), the integrated χ^2 is

$$\tilde{\chi}^2_{SN,GRB} = D - \frac{E^2}{F} + \ln\frac{F}{2\pi}, \tag{19}$$

for

$$D = \sum_i \left(\Delta\mu\, C_{cov}^{-1}\, \Delta\mu^T\right)^2, \tag{20a}$$

$$E = \sum_i \left(\Delta\mu\, C_{cov}^{-1}\, E\right), \tag{20b}$$

$$F = \sum_i C_{cov}^{-1}, \tag{20c}$$

where μ^i is the observed luminosity, σ_i is its error, $d_L(z)$ is the luminosity distance, $\Delta\mu = \mu^i - 5\log_{10}[d_L(z_i))$, E is the unit matrix, and C_{cov}^{-1} is the inverse covariance matrix of the dataset. For the GRB dataset, $C^{-1} \to 1/\sigma_i^2$ since there is no known covariance matrix for it. For the Pantheon dataset, the total covariance is defined as $C_{cov} = D_{stat} + C_{sys}$, where $D_{stat} = \sigma_i^2$ comes from the measurement and C_{sys} is provided separately [79]. Note, in the so-defined marginalized χ^2, the values of M and H_0 do not change the marginalized $\tilde{\chi}^2_{SN}$.

The final χ^2 is

$$\chi^2 = \chi^2_{BAO} + \chi^2_{CMB} + \chi^2_{SN} + \chi^2_{GRB}.$$

4. Datasets

The dataset we are using is a collection of points from different BAO observations [80–92], to which we add the CMB distant prior [57] and the data from the binned Pantheon dataset, which contain 1048 supernovae luminosity measurements in the redshift range $z \in (0.01, 2.3)$ [93] binned into 40 points. The GRB dataset [94] consists of 162 measurements in the range $z \in [0.03351, 9.3]$.

To estimate the possible correlations in the BAO dataset, we use the methodology in [95,96]. This method avoids the use of N-body mocks to find the covariance matrices due to systematic errors and replaces it with an evaluation of the effect of possible small correlation on the final result. We add to the covariance matrix for uncorrelated points $C_{ii} = \sigma_i^2$ symmetrically a number of randomly selected nondiagonal elements C_{ij}. Their magnitudes are set to $C_{ij} = 0.5\sigma_i\sigma_j$, where $\sigma_i\sigma_j$ are the published 1σ errors of the data points i, j. We introduce positive correlations in up to 6 pairs of randomly selected data points (more than 25% of the data). Figure A1 in Appendix A shows the corner plots with different randomized points for all the models we employ in this article. From the plots, one can see that the effect from adding the correlations is below 10% on average. This indicates that we can consider the chosen set of BAO points for being effectively uncorrelated.

To run the inference, we use a Monte Carlo Markov Chain (MCMC) nested sampler to find the best fit. We use the open-source package *Polychord* [97] with the *GetDist* package [98] to present the results.

The prior is a uniform distribution for all the quantities: $\Omega_m \in [0, 1.]$, $\Omega_\Lambda \in [0, 1 - \Omega_m]$, $\Omega_r \in [0, 1 - \Omega_m - \Omega_\Lambda]$, $c/(H_0 r_d) \in [25, 35]$, $w_0 \in [-1.5, -0.5]$ and $w_a \in [-0.5, 0.5]$. Since the distance prior is defined at the decoupling epoch (z_*) and the BAO—at drag epoch (z_d), we parametrize the difference between $r_s(z_*)$ and $r_s(z_d)$ as $rat = r_*/r_d$, where the prior for the ratio is $rat \in [0.9, 1.1]$.

5. Results

Figure 1 (as well as the figures in the Appendix A) show the final values obtained by running MCMC on the selected priors, the numbers being in Table A3 in the Appendix A, where also the corner plots can be found. We see that the models differ seriously in their estimations for the physical quantities $c/(H_0 r_d)$, Ω_m and r_d/r_s, probably due to the very wide prior imposed on Ω_m.

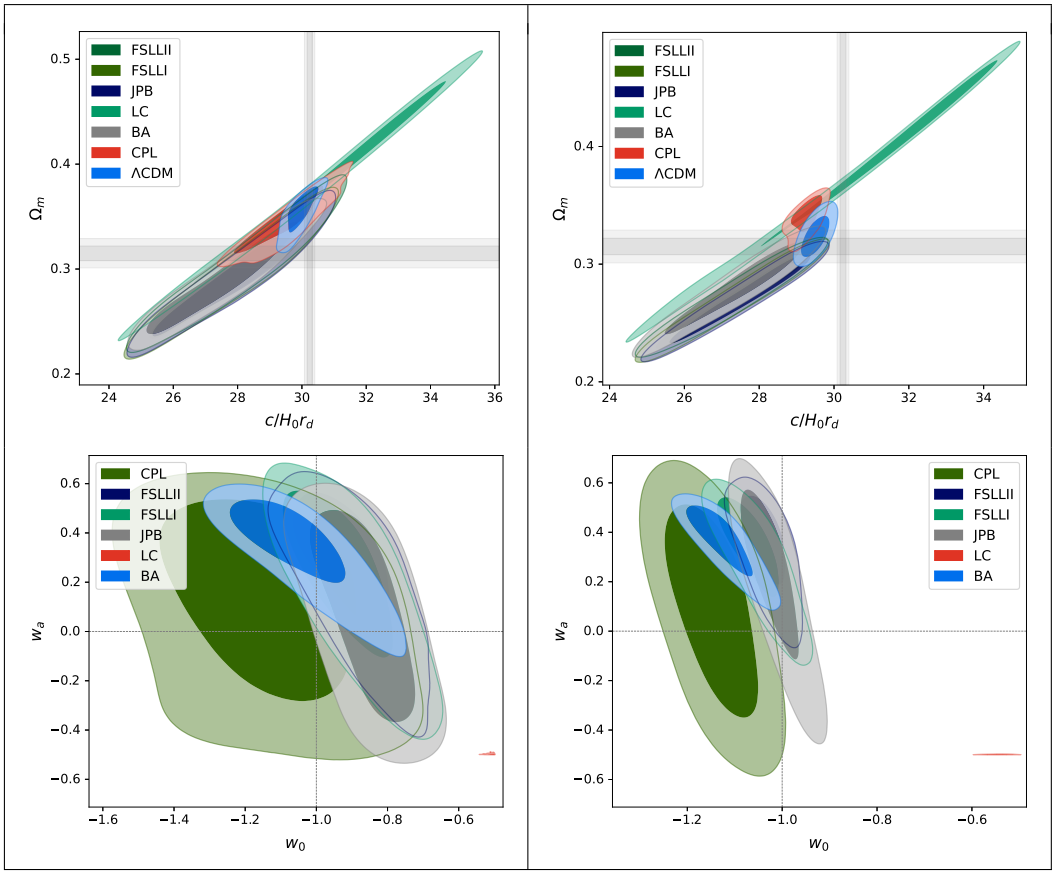

Figure 1. The 2D contour plot for the different DE parametrizations for the BAO+CMB dataset to the left and for the BAO+CMB+SN+GRB to the right. The upper panel shows the results for Ω_m vs. $c/(H_0 r_d)$ and the lower panel shows the results for w and w_a. ΛCDM corresponds to $w_0 = -1$ and $w_a = 0$. The grey lines show the 1σ and 2σ of Ω_m and $c/(H_0 r_d)$ as measured by Planck 2018, while on the bottom plot the gray cross shows where we recover ΛCDM.

Since we avoid the degeneracy between r_d and H_0 by considering the combined quantity $c/(H_0 r_d)$ this leads to an explicit correlation with Ω_m for some models and rather strict bounds on the error. The values of Ω_m closest to the ones published by Planck 2018 [7] $\Omega_m = 0.315 \pm 0.007$ are for the BA, JPB and FSLLI models for the BAO dataset and ΛCDM[1] and BA for the BAO+SN+GRB. The rest significantly overestimate Ω_m . For the ratio r_*/r_d Planck 2018 gives 0.98, the closest models are BA, JPB and FSLLI/FSLLII models for the BAO dataset and (flat) ΛCDM, JPB and FSLLI/FSLLII for the BAO+SN+GRB. For $c/(H_0 r_d)$, the Planck 2018 values is 30.26 ± 0.06. Here, the models closest to this value are ΛCDM, CPL and LC for the BAO dataset and ΛCDM, CPL and LC for the BAO+SN+GRB.

The DE parameters seem to be constrained to different level for the different models. As a whole, the trend to better constrain w_0 than w_a, which we observed in [46] (and the referenced inside other works), is confirmed in this case as well. Notable exceptions are the BA and LC models, where the error of w_a is much smaller. For them, however, the other parameters seem to be outside of the expected boundaries. ΛCDM performs as expected under both datasets.

To compare the different models, we use well-known statistical measures. The results can be seen in Table 1. In it, we publish four selection criteria: Akaike information criterion (AIC), Bayesian information criterion (BIC), deviance information criterion (DIC) and the Bayes factor (BF). Since for small datasets, both AIC and BIC are dominated by the number of parameters in the model (which are 3 for ΛCDM, and 5 for the DE models), we emphasize here on the DIC and the BF which rely on the numerically evaluated likelihood and evidence, making them more unbiased. The DIC criterion, just like the AIC, selects the

best model to be the one with the minimal value of the DIC measurement. The reference table we use for DIC is $\Delta DIC > 10$ shows strong support for the model with lower DIC, $\Delta DIC = 5$–10 shows substantial support for the model with lower DIC, and $\Delta DIC < 5$ gives ambiguous support for the model with lower DIC. Here, we use the logarithmic scale for the BF, for which $ln(BF) > 1$ shows support for the base model (ΛCDM), while $ln(BF) < -1$ for the other hypothesis. $|ln(BF)| < 1$ shows an inconclusive result.

Table 1. Selection criteria of different models in a comparison to the ΛCDM model for the BAO dataset and the BAO+SN+GRB dataset.

BAO+CMB							
Model	AIC	ΔAIC	BIC	ΔBIC	DIC	ΔDIC	ln(BF)
ΛCDM	22.0		24.5		16.8		
CPL	25.7	-3.7	29.9	-5.4	16.5	0.3	0.6
BA	25.3	-3.3	29.5	-4.9	16.2	0.65	-5.3
LC	56.0	-33.9	60.2	-35.6	51.1	-34.3	38.5
JPB	27.8	-5.8	31.9	-7.4	18.6	-1.8	-3.5
FSLLI	27.1	-5.1	31.3	-6.9	17.9	-1.1	-3.8
FSLLII	26.6	-4.6	30.8	-6.3	17.4	-0.65	-4.0
BAO+CMB+SN+GRB							
ΛCDM	228.1		238.3		222.7		
CPL	229.2	-1.1	246.1	-7.8	219.9	2.8	-1.2
BA	229.0	-0.9	246.0	-7.8	219.8	2.9	-5.9
LC	436.8	-208.7	453.7	-215.5	427.6	-204.9	208.9
JPB	232.2	-4.1	249.2	-10.9	222.9	-0.2	-4.0
FSLLI	231.1	-2.9	248.0	-9.7	221.9	0.9	-3.7
FSLLII	230.5	-2.4	247.4	-9.2	221.3	1.5	-4.8

From Table 1, we see that the AIC and BIC for all models show a preference for ΛCDM. For the DIC criterion, we see a slight possibility for a preference for other models in the case of the CPL and BA models for both tested datasets. For the BF, we see that there is some possible preference for BA, JPN and FSLLI/FSLLII for the BAO+CMB case and for CPL and BA, JPN and FSLLI/FSLLII in the BAO+CMB+SN+GRB case. The results of the LC model show that it is underfitting the data (from the $\chi^2/dof \sim 2$) and the statistics for it is not reliable. This demonstrates another benefit of performing the statistical analysis.

The preference for the BA and LC models which we observe was also observed in the results of [43], where the authors studied a dataset consisting of SN, cosmic chronometers and gravitational waves.

The BAO dataset we use combines the H_0 and the r_d into one quantity. Therefore, we estimate the new variable $c/(H_0 r_d) \sim 30$. Figure 2 shows the values of the $c/(H_0 r_d)$ for different models vs. the result from Planck 2018: 30.24 ± 0.08. For comparison, the most recent local measurement by SH0ES is 30.19 ± 0.53, corresponding to $H_0 = 73.01 \pm 0.99$ km s^{-1}Mpc^{-1} [5]. We do not put it on the plot, because the r_d used to obtain it is the indirect result from inference on the H0LiCOW+SN+BAO+SH0ES dataset [65]. It is, however, clearly very close to the Planck value, as expected.

On Figure 2, we superimpose the BAO+CMB-only result with the BAO+CMB+SN+GRB one. This figure enables us to visually track the tension between the Planck 2018 results and the datasets we use, which are mostly local universe ones (except for the 2 CMB points). We see that the tension is now between $c/(H_0 r_d)$ and Ω_m. The models whose bounds cross with the Planck 2018 one for $c/(H_0 r_d)$ are ΛCDM, CPL and LC for BAO+CMB and

only LC for the BAO+CMB+SN+GRB dataset. For Ω_m, the models that enter the interval are all but ΛCDM and CPL for the BAO+CMB dataset and ΛCDM, BA, LC for the BAO+CMB+SN+GRB dataset. We see that the inclusion of the new datasets decreases the number of models satisfying the constraints. The only model that is not in tension is LC because of its huge error. Notably, in this approach, ΛCDM, while satisfying the bounds for $c/(H_0 r_d)$, does not satisfy them for Ω_m.

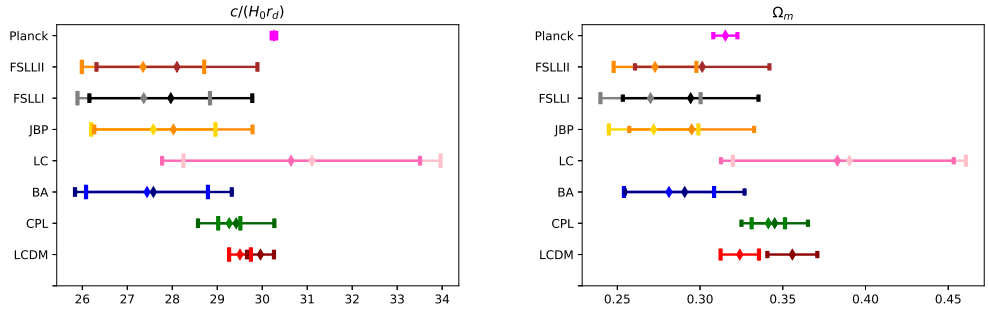

Figure 2. The final values of the $c/(H_0 r_d)$ from different DE models, compared to the values from Planck for the BAO+CMB+SN+GRB dataset. The smaller, darker, errorbox are for BAO+CMB, the lighter, bigger errorbox–for SN+GRB.

From the plot, one can see that in general adding the new datasets decrease the errors, but they do not move the mean values in the same direction and the overall effect is not very big. This may be due to unknown errors in the SN+GRB dataset or to the fact that this dataset is not sensitive toward the combined variable $c/(H_0 r_d)$ since we have marginalized over H_0 so that we do not have to impose a prior on r_d. Because of this, the only effect the SN+GRB dataset has on the combined variable is indirect, through Ω_m and the other parameters. It could also point to some inconsistency in the $\mu(M_B)$ relation such as the ones considered in [100–105]) questioning the assumption that $M_B = const.$

6. Discussion

This paper uses the combination $H_0 \cdot r_d$ to avoid the degeneracy between H_0 and r_d which has plagued the use of BAO measurements and could be part of the resolution of cosmological tensions. The use of a combined parameter avoids imposing separate priors on H_0 and r_d and thus it avoids additional assumptions on them. We use points from the late universe, the BAO dataset ($z < 2.4$)), few points from the early universe (the CMB distant priors, ($z \simeq 1089$)), to which we add SN data and GRB datasets, properly marginalized, to make a statistical comparison between different DE models.

The results show that the tension is now between the new parameter $c/(H_0 r_d)$ and Ω_m—the only model that fits in the constraints set by Planck 2018 is LC, which comes with the biggest error. For the rest of the models, one of the two parameters do not fit the constraints, even if some of them somewhat reduce the tension. Statistically, there is a preference for the ΛCDM model over the DE models in most cases. It is worth noting that there is strong evidence in support of ΛCDM compared to all other models only when using AIC and BIC, while from DIC and BF, the support is not substantial, and it even slightly favors other models. This result raises the question of the use of different statistical measures when comparing DE models, and also it opens the possibility that a better DE model may eventually help in reducing both the H_0 tension and the r_d tension.

Another interesting point is that for some models, the known impossibility to constrain w_a is eliminated and w_a has very tight bounds. These models, LC and BA and somewhat FSLLI, show interesting new possibilities for DE models. Furthermore, the choice of datasets and models make explicit the degeneracy between $H_0 \cdot r_d$ and Ω_m, emphasizing the need to find a way to disentangle the three quantities—H_0, r_d and Ω_m—if we are to understand the cosmological tensions. The results show that adding the SN and GRB datasets decrease the errors on the constrained parameters, but they do not move them in

the same direction for each model. We see that combining different datasets and different marginalization techniques, along with the use of statistical measures, is a promising tool to study new cosmological models.

Funding: Bulgarian National Science Fund research grants KP-06-N58/5/19 December 2021.

Data Availability Statement: All the data we used in this paper were taken from the corresponding citations and available to use.

Acknowledgments: D.S. thanks David Benisty for the useful comments and discussions. D.S. is thankful to Bulgarian National Science Fund for support via research grants KP-06-N58/5.

Conflicts of Interest: The authors declare no conflict of interest.

Appendix A. Some Extra Material

Table A1. The uncorrelated dataset used in this paper. For each redshift, the table presents the parameter, the mean value, and the corresponding error bar. The reference and the collaboration are also reported.

z	D_A/r_d	Error	Year	Survey	Ref.
0.11	2.607	0.138	2021	SDSS blue galaxies	[106]
0.24	5.594	0.305	2016	BOSS-DR12 RSD of LOWZ and CMASS	[88]
0.32	6.636	0.11	2016	SDSS-DR9+DR10+DR11+DR12 +covariance	[89]
0.38	7.389	0.122	2019	BOSS-DR12 power spectrum	[90]
0.44	8.19	0.77	2012	WiggleZ (galaxy clustering)	[80]
0.54	9.212	0.41	2012	SDSS-III DR8 (luminous galaxies)	[82]
0.6	9.37	0.65	2012	WiggleZ (galaxy clustering)	[80]
0.697	10.18	0.52	2020	DECals DR8 (LRG)	[83]
0.73	10.42	0.73	2012	Wiggle (galaxy clustering)	[80]
0.81	10.75	0.43	2017	DES Year1 (galaxy clustering)	[91]
0.85	10.76	0.54	2020	eBOSS DR16 ELG	[84]
0.874	11.41	0.74	2020	DECals DR8 (LRG)	[83]
1.00	11.521	1.032	2019	eBOSS DR14 quasar clustering	[85]
2.00	12.011	0.562	2019	eBOSS DR14 quasars clustering	[85]
2.35	10.83	0.54	2019	BOSS DR14 Lya and quasars	[87]
2.4	10.5	0.34	2017	SDSS-III/DR12	[92]

Table A2. The 68 % C.L. limits for R, l_A, in different cosmological models and their correlation matrix for from Planck 2018 TT,TE,EE+lowE; see the text for details.

ΛCDM	Planck TT,TE,EE + lowE	R	$l_{\rm A}$
R	1.7502 ± 0.0046	1.0	0.46
$l_{\rm A}$	$301.471^{+0.089}_{-0.090}$	0.46	1.0
wCDM	Planck TT,TE,EE + lowE	R	$l_{\rm A}$
R	$1.7493^{+0.0046}_{-0.0047}$	1.0	0.47
$l_{\rm A}$	$301.462^{+0.089}_{-0.090}$	0.47	1.0
$\Omega_k\Lambda$CDM	Planck TT,TE,EE + lowE	R	$l_{\rm A}$
R	1.7429 ± 0.0051	1.0	0.54
$l_{\rm A}$	301.409 ± 0.091	0.54	1.0

Table A3. The posterior values for $c/(H_0 r_d)$, Ω_m, r_*/r_d and w_0, w_a for different parametrization of DE for the BAO+CMB dataset (top) and for the BAO+CMB+SN+GRB (bottom).

BAO+CMB					
Model	$c/(H_0 r_d)$	Ω_m	r_*/r_d	w	w_a
ΛCDM	29.96 ± 0.3	0.36 ± 0.02	0.92 ± 0.01	-1.000	0.000
CPL	29.42 ± 0.85	0.35 ± 0.02	0.91 ± 0.01	-1.14 ± 0.19	0.13 ± 0.31
BA	27.58 ± 1.74	0.29 ± 0.04	0.93 ± 0.02	-1.06 ± 0.11	0.35 ± 0.12
LC	30.64 ± 2.87	0.38 ± 0.07	0.901 ± 0.0009	-0.5082 ± 0.0072	-0.4979 ± 0.0018
JPB	28.03 ± 1.76	0.29 ± 0.04	0.94 ± 0.02	-0.86 ± 0.09	0.08 ± 0.31
FSLLI	27.97 ± 1.81	0.29 ± 0.04	0.94 ± 0.02	-0.92 ± 0.1	0.22 ± 0.24
FSLLII	28.1 ± 1.79	0.3 ± 0.04	0.94 ± 0.02	-0.91 ± 0.09	0.26 ± 0.2
BAO+CMB+SN+GRB					
ΛCDM	29.51 ± 0.24	0.32 ± 0.01	0.95 ± 0.01	-1.000	0.000
CPL	29.27 ± 0.25	0.34 ± 0.01	0.91 ± 0.01	-1.15 ± 0.06	0.09 ± 0.31
BA	27.44 ± 1.36	0.28 ± 0.03	0.94 ± 0.01	-1.13 ± 0.04	0.37 ± 0.1
LC	31.11 ± 2.86	0.39 ± 0.07	0.9009 ± 0.0007	-0.55 ± 0.02	-0.4992 ± 0.0007
JPB	27.58 ± 1.38	0.27 ± 0.03	0.9657 ± 0.0084	-1.02 ± 0.04	0.22 ± 0.23
FSLLI	27.37 ± 1.47	0.27 ± 0.03	0.9614 ± 0.0082	-1.06 ± 0.04	0.32 ± 0.14
FSLLII	27.35 ± 1.36	0.27 ± 0.03	0.9556 ± 0.0099	-1.04 ± 0.03	0.35 ± 0.13

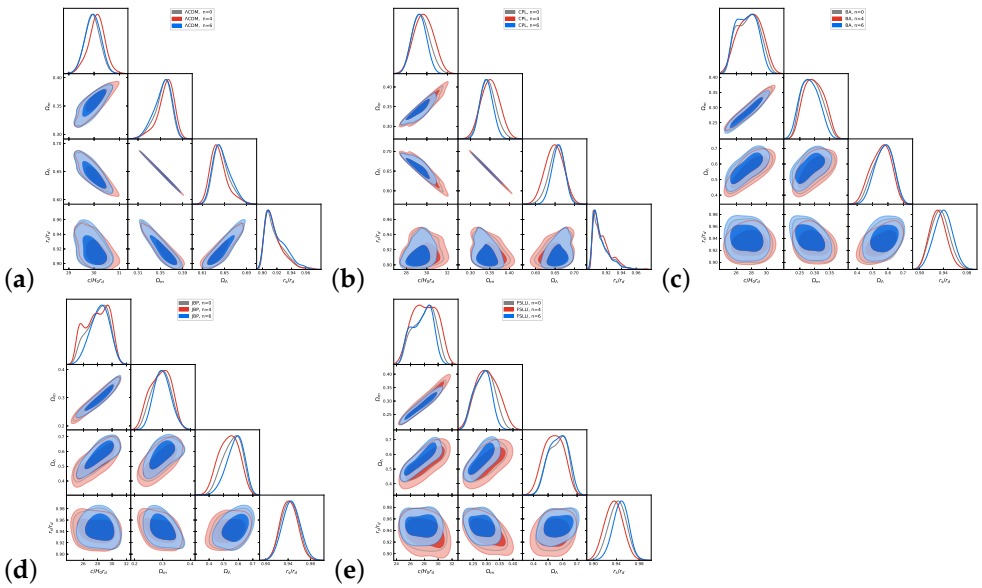

Figure A1. The covariance test plot for the considered models: (**a**) ΛCDM, (**b**) *CPL*, (**c**) *BA*, (**d**) *JPB*, (**e**) *FSLLI* model.

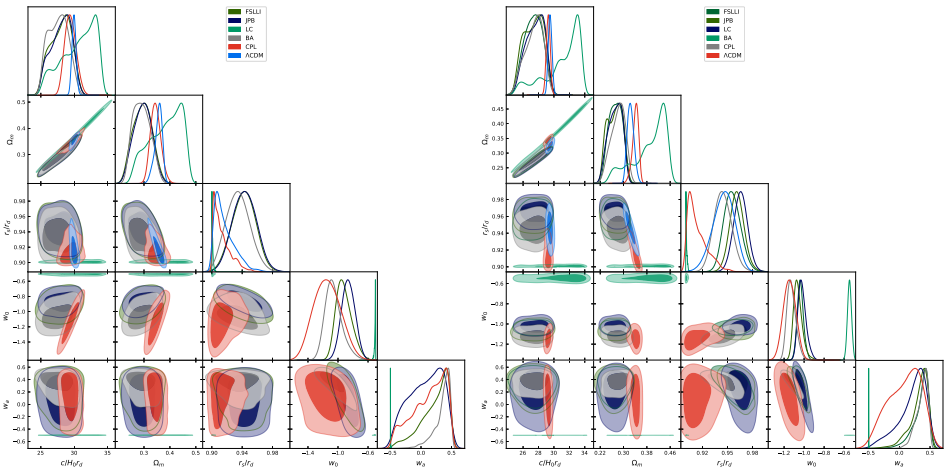

Figure A2. The posterior distribution for $c/(H_0 r_d)$, Ω_m, r_*/r_d and w_0, w_a for different parametrization of DE for the BAO+CMB dataset to the left and for the BAO+CMB+SN+GRB to the right.

Notes

[1] In Sections 5 and 6 we discuss only the **flat** ΛCDM model. The effect of the spatial curvature on DE models has been considered recently in [99].

References

1. Freedman, W.L.; Madore, B.F.; Gibson, B.K.; Ferrarese, L.; Kelson, D.D.; Sakai, S.; Mould, J.R.; Kennicutt, J.R.C.; Ford, H.C.; Graham, J.A.; et al. Final results from the Hubble Space Telescope key project to measure the Hubble constant. *Astrophys. J.* **2001**, *553*, 47–72. [CrossRef]
2. Riess, A.G.; Filippenko, A.V.; Challis, P.; Clocchiatti, A.; Diercks, A.; Garnavich, P.M.; Gilliland, R.L.; Hogan, C.J.; Jha, S.; Kirshner, R.P.; et al. Observational evidence from supernovae for an accelerating universe and a cosmological constant. *Astron. J.* **1998**, *116*, 1009–1038. [CrossRef]
3. Perlmutter, S.; Aldering, G.; Goldhaber, G.; Knop, R.A.; Nugent, P.; Castro, P.G.; Deustua, S.; Fabbro, S.; Goobar, A.; Groom, D.E.; et al. Measurements of Ω and Λ from 42 high redshift supernovae. *Astrophys. J.* **1999**, *517*, 565–586. [CrossRef]
4. Riess, A.G.; Casertano, S.; Yuan, W.; Bowers, J.B.; Macri, L.; Zinn, J.C.; Scolnic, D. Cosmic Distances Calibrated to 1% Precision with Gaia EDR3 Parallaxes and Hubble Space Telescope Photometry of 75 Milky Way Cepheids Confirm Tension with ΛCDM. *Astrophys. J. Lett.* **2021**, *908*, L6. [CrossRef]
5. Riess, A.G.; Breuval, L.; Yuan, W.; Casertano, S.; Macri, L.M.; Scolnic, D.; Cantat-Gaudin, T.; Anderson, R.I.; Reyes, M.C. Cluster Cepheids with High Precision Gaia Parallaxes, Low Zeropoint Uncertainties, and Hubble Space Telescope Photometry. *arXiv* **2022**, arXiv:2208.01045.
6. Troxel, M.A.; MacCrann, N.; Zuntz, J.; Eifler, T.F.; Krause, E.; Dodelson, S.; Gruen, D.; Blazek, J.; Friedrich, O.; Samuroff, S.; et al. Dark Energy Survey Year 1 results: Cosmological constraints from cosmic shear. *Phys. Rev. D* **2018**, *98*, 043528. [CrossRef]
7. Aghanim, N.; Akrami, Y.; Ashdown, M.; Aumont, J.; Baccigalupi, C.; Ballardini, M.; Banday, A.J.; Barreiro, R.B.; Bartolo, N.; Basak, S.; et al. Planck 2018 results. VI. Cosmological parameters. *Astron. Astrophys.* **2020**, *641*, A6. [CrossRef]
8. Ade, P.A.R.; Aghanim, N.; Arnaud, M.; Ashdown, M.; Aumont, J.; Baccigalupi, C.; Banday, A.J.; Barreiro, R.B.; Bartlett, J.G.; Bartolo, N.; et al. Planck 2015 results. XIII. Cosmological parameters. *Astron. Astrophys.* **2016**, *594*, A13. [CrossRef]
9. Dainotti, M.G.; De Simone, B.; Schiavone, T.; Montani, G.; Rinaldi, E.; Lambiase, G. On the Hubble constant tension in the SNe Ia Pantheon sample. *Astrophys. J.* **2021**, *912*, 150. [CrossRef]
10. Benisty, D.; Vasak, D.; Kirsch, J.; Struckmeier, J. Low-redshift constraints on covariant canonical Gauge theory of gravity. *Eur. Phys. J. C* **2021**, *81*, 125. [CrossRef]
11. Capozziello, S.; De Laurentis, M. Extended Theories of Gravity. *Phys. Rept.* **2011**, *509*, 167–321. [CrossRef]
12. Bull, P.; Akrami, Y.; Adamek, J.; Baker, T.; Bellini, E.; Jimenez, J.B.; Bentivegna, E.; Camera, S.; Clesse, S.; Davis, J.H.; et al. Beyond ΛCDM: Problems, solutions, and the road ahead. *Phys. Dark Univ.* **2016**, *12*, 56–99. [CrossRef]
13. Di Valentino, E.; Mena, O.; Pan, S.; Visinelli, L.; Yang, W.; Melchiorri, A.; Mota, D.F.; Riess, A.G.; Silk, J. In the Realm of the Hubble tension—A Review of Solutions. *arXiv* **2021**, arXiv:2103.01183.
14. Yang, W.; Di Valentino, E.; Pan, S.; Wu, Y.; Lu, J. Dynamical dark energy after Planck CMB final release and H_0 tension. *Mon. Not. Roy. Astron. Soc.* **2021**, *501*, 5845–5858. [CrossRef]
15. Schöneberg, N.; Lesgourgues, J.; Hooper, D.C. The BAO+BBN take on the Hubble tension. *JCAP* **2019**, *10*, 029. [CrossRef]
16. Di Valentino, E. Crack in the cosmological paradigm. *Nat. Astron.* **2017**, *1*, 569–570. [CrossRef]
17. Di Valentino, E.; Anchordoqui, L.A.; Akarsu, O.; Ali-Haimoud, Y.; Amendola, L.; Arendse, N.; Asgari, M.; Ballardini, M.; Basilakos, S.; Battistelli, E.; et al. Cosmology Intertwined II: The Hubble Constant Tension. *arXiv* **2020**, arXiv:2008.11284.

18. Perivolaropoulos, L.; Skara, F. Challenges for ΛCDM: An update. *arXiv* **2021**, arXiv:2105.05208.
19. Lucca, M. Dark energy-dark matter interactions as a solution to the S_8 tension. *arXiv* **2021**, arXiv:2105.09249.
20. Colgáin, E.O.; Sheikh-Jabbari, M.M.; Solomon, R.; Bargiacchi, G.; Capozziello, S.; Dainotti, M.G.; Stojkovic, D. Revealing intrinsic flat ΛCDM biases with standardizable candles. *Phys. Rev. D* **2022**, *106*, L041301. [CrossRef]
21. Colgáin, E.O.; Sheikh-Jabbari, M.M.; Solomon, R.; Dainotti, M.G.; Stojkovic, D. Putting Flat ΛCDM In The (Redshift) Bin. *arXiv* **2022**, arXiv:2206.11447.
22. Wang, Y.; Pogosian, L.; Zhao, G.B.; Zucca, A. Evolution of dark energy reconstructed from the latest observations. *Astrophys. J. Lett.* **2018**, *869*, L8. [CrossRef]
23. Reyes, M.; Escamilla-Rivera, C. Improving data-driven model-independent reconstructions and new constraints in Horndeski cosmology. *arXiv* **2021**, arXiv:2104.04484.
24. Colgáin, E.Ó.; Sheikh-Jabbari, M.M.; Yin, L. Can dark energy be dynamical? *arXiv* **2021**, arXiv:2104.01930.
25. Liu, W.; Anchordoqui, L.A.; Di Valentino, E.; Pan, S.; Wu, Y.; Yang, W. Constraints from High-Precision Measurements of the Cosmic Microwave Background: The Case of Disintegrating Dark Matter with Λ or Dynamical Dark Energy. *arXiv* **2021**, arXiv:2108.04188.
26. Pettorino, V.; Amendola, L.; Wetterich, C. How early is early dark energy? *Phys. Rev. D* **2013**, *87*, 083009. [CrossRef]
27. Poulin, V.; Smith, T.L.; Karwal, T.; Kamionkowski, M. Early Dark Energy Can Resolve The Hubble Tension. *Phys. Rev. Lett.* **2019**, *122*, 221301. [CrossRef] [PubMed]
28. Lin, M.X.; Hu, W.; Raveri, M. Testing H_0 in Acoustic Dark Energy with Planck and ACT Polarization. *Phys. Rev. D* **2020**, *102*, 123523. [CrossRef]
29. Smith, T.L.; Lucca, M.; Poulin, V.; Abellan, G.F.; Balkenhol, L.; Benabed, K.; Galli, S.; Murgia, R. Hints of early dark energy in Planck, SPT, and ACT data: New physics or systematics? *Phys. Rev. D* **2022**, *106*, 043526. [CrossRef]
30. Smith, T.L.; Poulin, V.; Bernal, J.L.; Boddy, K.K.; Kamionkowski, M.; Murgia, R. Early dark energy is not excluded by current large-scale structure data. *Phys. Rev. D* **2021**, *103*, 123542. [CrossRef]
31. Di Valentino, E. A combined analysis of the H_0 late time direct measurements and the impact on the Dark Energy sector. *Mon. Not. Roy. Astron. Soc.* **2021**, *502*, 2065–2073. [CrossRef]
32. Haridasu, B.S.; Viel, M.; Vittorio, N. Sources of H_0-tension in dark energy scenarios. *Phys. Rev. D* **2021**, *103*, 063539. [CrossRef]
33. Li, X.; Shafieloo, A. A Simple Phenomenological Emergent Dark Energy Model can Resolve the Hubble Tension. *Astrophys. J. Lett.* **2019**, *883*, L3. [CrossRef]
34. Yang, W.; Di Valentino, E.; Pan, S.; Mena, O. Emergent Dark Energy, neutrinos and cosmological tensions. *Phys. Dark Univ.* **2021**, *31*, 100762. [CrossRef]
35. Kumar, S.; Nunes, R.C. Echo of interactions in the dark sector. *Phys. Rev. D* **2017**, *96*, 103511. [CrossRef]
36. Di Valentino, E.; Melchiorri, A.; Mena, O.; Vagnozzi, S. Interacting dark energy in the early 2020s: A promising solution to the H_0 and cosmic shear tensions. *Phys. Dark Univ.* **2020**, *30*, 100666. [CrossRef]
37. Yang, W.; Mena, O.; Pan, S.; Di Valentino, E. Dark sectors with dynamical coupling. *Phys. Rev. D* **2019**, *100*, 083509. [CrossRef]
38. Gogoi, A.; Sharma, R.K.; Chanda, P.; Das, S. Early Mass-varying Neutrino Dark Energy: Nugget Formation and Hubble Anomaly. *Astrophys. J.* **2021**, *915*, 132. [CrossRef]
39. Sakstein, J.; Trodden, M. Early Dark Energy from Massive Neutrinos as a Natural Resolution of the Hubble Tension. *Phys. Rev. Lett.* **2020**, *124*, 161301. [CrossRef]
40. Tian, S.X.; Zhu, Z.H. Early dark energy in *k*-essence. *Phys. Rev. D* **2021**, *103*, 043518. [CrossRef]
41. Nojiri, S.; Odintsov, S.D.; Saez-Chillon Gomez, D.; Sharov, G.S. Modelling and testing the equation of state for (Early) dark energy. *arXiv* **2021**, arXiv:2103.05304.
42. Seto, O.; Toda, Y. Comparing early dark energy and extra radiation solutions to the Hubble tension with BBN. *Phys. Rev. D* **2021**, *103*, 123501. [CrossRef]
43. Escamilla-Rivera, C.; Nájera, A. Dynamical dark energy models in the light of gravitational-wave transient catalogues. *JCAP* **2022**, *03*, 060. [CrossRef]
44. Motta, V.; García-Aspeitia, M.A.; Hernández-Almada, A.; Magaña, J.; Verdugo, T. Taxonomy of Dark Energy Models. *Universe* **2021**, *7*, 163. [CrossRef]
45. Yang, W.; Di Valentino, E.; Pan, S.; Shafieloo, A.; Li, X. Generalized emergent dark energy model and the Hubble constant tension. *Phys. Rev. D* **2021**, *104*, 063521. [CrossRef]
46. Staicova, D.; Benisty, D. Constraining the dark energy models using Baryon Acoustic Oscillations: An approach independent of $H_0 \cdot r_d$. *arXiv* **2021**, arXiv:2107.14129.
47. Aubourg, E.; Bailey, S.; Bautista, J.E.; Beutler, F.; Bhardwaj, V.; Bizyaev, D.; Blanton, M.; Blomqvist, M.; Bolton, A.S.; Bovy, J.; et al. Cosmological implications of baryon acoustic oscillation measurements. *Phys. Rev. D* **2015**, *92*, 123516. [CrossRef]
48. Arendse, N.; Agnello, A.; Wojtak, R. Low-redshift measurement of the sound horizon through gravitational time-delays. *Astron. Astrophys.* **2019**, *632*, A91. [CrossRef]
49. Aylor, K.; Joy, M.; Knox, L.; Millea, M.; Raghunathan, S.; Wu, W.L.K. Sounds Discordant: Classical Distance Ladder & ΛCDM -based Determinations of the Cosmological Sound Horizon. *Astrophys. J.* **2019**, *874*, 4. [CrossRef]
50. Pogosian, L.; Zhao, G.B.; Jedamzik, K. Recombination-independent determination of the sound horizon and the Hubble constant from BAO. *Astrophys. J. Lett.* **2020**, *904*, L17. [CrossRef]

51. Aizpuru, A.; Arjona, R.; Nesseris, S. Machine learning improved fits of the sound horizon at the baryon drag epoch. *Phys. Rev. D* **2021**, *104*, 043521. [CrossRef]
52. Jedamzik, K.; Pogosian, L.; Zhao, G.B. Why reducing the cosmic sound horizon alone can not fully resolve the Hubble tension. *Commun. Phys.* **2021**, *4*, 123. [CrossRef]
53. de la Macorra, A.; Almaraz, E.; Garrido, J. Towards a Solution to the H0 Tension: The Price to Pay. *arXiv* **2021**, arXiv:2106.12116.
54. Wang, Y.; Wang, S. Distance Priors from Planck and Dark Energy Constraints from Current Data. *Phys. Rev. D* **2013**, *88*, 043522; Erratum in *Phys. Rev. D* **2013**, *88*, 069903[CrossRef]
55. Mamon, A.A.; Bamba, K.; Das, S. Constraints on reconstructed dark energy model from SN Ia and BAO/CMB observations. *Eur. Phys. J. C* **2017**, *77*, 29. [CrossRef]
56. Grandon, D.; Cardenas, V.H. Exploring evidence of interaction between dark energy and dark matter. *arXiv* **2018**, arXiv:1804.03296.
57. Chen, L.; Huang, Q.G.; Wang, K. Distance Priors from Planck Final Release. *JCAP* **2019**, *02*, 028. [CrossRef]
58. da Silva, W.J.C.; Silva, R. Extended ΛCDM model and viscous dark energy: A Bayesian analysis. *JCAP* **2019**, *05*, 036. [CrossRef]
59. Zhai, Z.; Wang, Y. Robust and model-independent cosmological constraints from distance measurements. *JCAP* **2019**, *07*, 005. [CrossRef]
60. Di Valentino, E.; Melchiorri, A.; Silk, J. Investigating Cosmic Discordance. *Astrophys. J. Lett.* **2021**, *908*, L9. [CrossRef]
61. Nilsson, N.A.; Park, M.I. Tests of standard cosmology in Hořava gravity, Bayesian evidence for a closed universe, and the Hubble tension. *Eur. Phys. J. C* **2022**, *82*, 873. [CrossRef]
62. Yao, Y.H.; Meng, X.H. Can interacting dark energy with dynamical coupling resolve the Hubble tension. *arXiv* **2022**, arXiv:2207.05955.
63. L'Huillier, B.; Shafieloo, A. Model-independent test of the FLRW metric, the flatness of the Universe, and non-local measurement of $H_0 r_d$. *JCAP* **2017**, *01*, 015. [CrossRef]
64. Shafieloo, A.; L'Huillier, B.; Starobinsky, A.A. Falsifying ΛCDM: Model-independent tests of the concordance model with eBOSS DR14Q and Pantheon. *Phys. Rev. D* **2018**, *98*, 083526. [CrossRef]
65. Arendse, N.; Wojtak, R.; Agnello, A.; Chen, G.C.-F.; Fassnacht, C.D.; Sluse, D.; Hilbert, S.; Millon, M.; Bonvin, V.; Wong, K.C.; et al. Cosmic dissonance: Are new physics or systematics behind a short sound horizon? *Astron. Astrophys.* **2020**, *639*, A57. [CrossRef]
66. Knox, L.; Millea, M. Hubble constant hunter's guide. *Phys. Rev. D* **2020**, *101*, 043533. [CrossRef]
67. Chevallier, M.; Polarski, D. Accelerating universes with scaling dark matter. *Int. J. Mod. Phys. D* **2001**, *10*, 213–224. [CrossRef]
68. Linder, E.V.; Huterer, D. How many dark energy parameters? *Phys. Rev. D* **2005**, *72*, 043509. [CrossRef]
69. Barger, V.; Guarnaccia, E.; Marfatia, D. Classification of dark energy models in the (w(0), w(a)) plane. *Phys. Lett. B* **2006**, *635*, 61–65. [CrossRef]
70. Barboza, E.M., Jr.; Alcaniz, J.S. A parametric model for dark energy. *Phys. Lett. B* **2008**, *666*, 415–419. [CrossRef]
71. Wang, Y. Figure of Merit for Dark Energy Constraints from Current Observational Data. *Phys. Rev. D* **2008**, *77*, 123525. [CrossRef]
72. Jassal, H.K.; Bagla, J.S.; Padmanabhan, T. WMAP constraints on low redshift evolution of dark energy. *Mon. Not. Roy. Astron. Soc.* **2005**, *356*, L11–L16. [CrossRef]
73. Feng, C.J.; Shen, X.Y.; Li, P.; Li, X.Z. A New Class of Parametrization for Dark Energy without Divergence. *JCAP* **2012**, *09*, 023. [CrossRef]
74. Komatsu, E.; Dunkley, J.; Nolta, M.R.; Bennett, C.L.; Gold, B.; Hinshaw, G.; Jarosik, N.; Larson, D.; Limon, M.; Page, L.; et al. Five-Year Wilkinson Microwave Anisotropy Probe (WMAP) Observations: Cosmological Interpretation. *Astrophys. J. Suppl.* **2009**, *180*, 330–376. [CrossRef]
75. Di Pietro, E.; Claeskens, J.F. Future supernovae data and quintessence models. *Mon. Not. Roy. Astron. Soc.* **2003**, *341*, 1299. [CrossRef]
76. Nesseris, S.; Perivolaropoulos, L. A Comparison of cosmological models using recent supernova data. *Phys. Rev. D* **2004**, *70*, 043531. [CrossRef]
77. Perivolaropoulos, L. Constraints on linear negative potentials in quintessence and phantom models from recent supernova data. *Phys. Rev. D* **2005**, *71*, 063503. [CrossRef]
78. Lazkoz, R.; Nesseris, S.; Perivolaropoulos, L. Exploring Cosmological Expansion Parametrizations with the Gold SnIa Dataset. *JCAP* **2005**, *11*, 010. [CrossRef]
79. Deng, H.K.; Wei, H. Null signal for the cosmic anisotropy in the Pantheon supernovae data. *Eur. Phys. J. C* **2018**, *78*, 755. [CrossRef]
80. Blake, C.; Brough, S.; Colless, M.; Contreras, C.; Couch, W.; Croom, S.; Croton, D.; Davis, T.M.; Drinkwater, M.J.; Forster, K.; et al. The WiggleZ Dark Energy Survey: Joint measurements of the expansion and growth history at $z < 1$. *Mon. Not. Roy. Astron. Soc.* **2012**, *425*, 405–414. [CrossRef]
81. Carvalho, G.C.; Bernui, A.; Benetti, M.; Carvalho, J.C.; Alcaniz, J.S. Baryon Acoustic Oscillations from the SDSS DR10 galaxies angular correlation function. *Phys. Rev. D* **2016**, *93*, 023530. [CrossRef]
82. Seo, H.-J.; Ho, S.; White, M.; Cuesta, A.J.; Ross, A.; Saito, S.; Reid, B.; Padmanabhan, N.; Percival, W.J.; De Putter, R.; et al. Acoustic scale from the angular power spectra of SDSS-III DR8 photometric luminous galaxies. *Astrophys. J.* **2012**, *761*, 13. [CrossRef]

83. Sridhar, S.; Song, Y.S.; Ross, A.J.; Zhou, R.; Newman, J.A.; Chuang, C.H.; Prada, F.; Blum, R.; Gaztañaga, E.; Landriau, M. Clustering of LRGs in the DECaLS DR8 Footprint: Distance Constraints from Baryon Acoustic Oscillations Using Photometric Redshifts. *Astrophys. J.* **2020**, *904*, 69. [CrossRef]
84. Tamone, A.; Raichoor, A.; Zhao, C.; de Mattia, A.; Gorgoni, C.; Burtin, E.; Ruhlmann-Kleider, V.; Ross, A.J.; Alam, S.; Percival, W.J.; et al. The Completed SDSS-IV extended Baryon Oscillation Spectroscopic Survey: Growth rate of structure measurement from anisotropic clustering analysis in configuration space between redshift 0.6 and 1.1 for the Emission Line Galaxy sample. *Mon. Not. Roy. Astron. Soc.* **2020**, *499*, 5527–5546. [CrossRef]
85. Zhu, F.; Padmanabhan, N.; Ross, A.J.; White, M.; Percival, W.J.; Ruggeri, R.; Zhao, G.; Wang, D.; Mueller, E.-M.; Burtin, E.; et al. The clustering of theSDSS-IV extended Baryon Oscillation Spectroscopic Survey DR14 quasar sample: Measuring the anisotropic baryon acoustic oscillations with redshift weights. *Mon. Not. Roy. Astron. Soc.* **2018**, *480*, 1096–1105. [CrossRef]
86. Hou, J.; Sánchez, A.G.; Ross, A.J.; Smith, A.; Neveux, R.; Bautista, J.; Burtin, E.; Zhao, C.; Scoccimarro, R.; Dawson, K.S.; et al. The Completed SDSS-IV extended Baryon Oscillation Spectroscopic Survey: BAO and RSD measurements from anisotropic clustering analysis of the Quasar Sample in configuration space between redshift 0.8 and 2.2. *Mon. Not. Roy. Astron. Soc.* **2020**, *500*, 1201–1221. [CrossRef]
87. Blomqvist, M.; Des Bourboux, H.D.M.; Busca, N.G.; de Sainte Agathe, V.; Rich, J.; Balland, C.; Bautista, J.E.; Dawson, K.; Font-Ribera, A.; Guy, J.; et al. Baryon acoustic oscillations from the cross-correlation of Lyα absorption and quasars in eBOSS DR14. *Astron. Astrophys.* **2019**, *629*, A86. [CrossRef]
88. Chuang, C.H.; Pellejero-Ibanez, M.; Rodríguez-Torres, S.; Ross, A.J.; Zhao, G.; Wang, Y.; Cuesta, A.J.; Rubiño-Martin, J.A.; Prada, F.; Alam, S.; et al. The clustering of galaxies in the completed SDSS-III Baryon Oscillation Spectroscopic Survey: Single-probe measurements from DR12 galaxy clustering—Towards an accurate model. *Mon. Not. Roy. Astron. Soc.* **2017**, *471*, 2370–2390. [CrossRef]
89. Alam, S.; Ata, M.; Bailey, S.; Beutler, F.; Bizyaev, D.; Blazek, J.A.; Bolton, A.S.; Brownstein, J.R.; Burden, A.; Chuang, C.-H.; et al. The clustering of galaxies in the completed SDSS-III Baryon Oscillation Spectroscopic Survey: Cosmological analysis of the DR12 galaxy sample. *Mon. Not. Roy. Astron. Soc.* **2017**, *470*, 2617–2652. [CrossRef]
90. Beutler, F.; Seo, H.-J.; Ross, A.J.; McDonald, P.; Saito, S.; Bolton, A.S.; Brownstein, J.R.; Chuang, C.-H.; Cuesta, A.J.; Eisenstein, D.J.; et al. The clustering of galaxies in the completed SDSS-III Baryon Oscillation Spectroscopic Survey: Baryon acoustic oscillations in the Fourier space. *Mon. Not. Roy. Astron. Soc.* **2017**, *464*, 3409–3430. [CrossRef]
91. Abbott, T.M.C.; Abdalla, F.B.; Alarcon, A.; Allam, S.; Andrade-Oliveira, F.; Annis, J.; Avila, S.; Banerji, M.; Banik, N.; Bechtol, K.; et al. Dark Energy Survey Year 1 Results: Measurement of the Baryon Acoustic Oscillation scale in the distribution of galaxies to redshift 1. *Mon. Not. Roy. Astron. Soc.* **2019**, *483*, 4866–4883. [CrossRef]
92. du Mas des Bourboux, H.; Le Goff, J.-M.; Blomqvist, M.; Busca, N.G.; Guy, J.; Rich, J.; Yèche, C.; Bautista, J.E.; Burtin, E.; Dawson, K.S.; et al. Baryon acoustic oscillations from the complete SDSS-III Lyα-quasar cross-correlation function at $z = 2.4$. *Astron. Astrophys.* **2017**, *608*, A130. [CrossRef]
93. Scolnic , D.M.; Jones, D.O.; Rest, A.; Pan, Y.C.; Chornock, R.; Foley, R.J.; Huber, M.E.; Kessler, R.; Narayan, G.; Riess, A.G.; et al. The Complete Light-curve Sample of Spectroscopically Confirmed SNe Ia from Pan-STARRS1 and Cosmological Constraints from the Combined Pantheon Sample. *Astrophys. J.* **2018**, *859*, 101. [CrossRef]
94. Demianski, M.; Piedipalumbo, E.; Sawant, D.; Amati, L. Cosmology with gamma-ray bursts: I. The Hubble diagram through the calibrated $E_{\rm p,i}$ - $E_{\rm iso}$ correlation. *Astron. Astrophys.* **2017**, *598*, A112. [CrossRef]
95. Kazantzidis, L.; Perivolaropoulos, L. Evolution of the $f\sigma_8$ tension with the Planck15/ΛCDM determination and implications for modified gravity theories. *Phys. Rev. D* **2018**, *97*, 103503. [CrossRef]
96. Benisty, D.; Staicova, D. Testing late-time cosmic acceleration with uncorrelated baryon acoustic oscillation dataset. *Astron. Astrophys.* **2021**, *647*, A38. [CrossRef]
97. Handley, W.J.; Hobson, M.P.; Lasenby, A.N. PolyChord: Nested sampling for cosmology. *Mon. Not. Roy. Astron. Soc.* **2015**, *450*, L61–L65. [CrossRef]
98. Lewis, A. GetDist: A Python package for analysing Monte Carlo samples. *arXiv* **2019**, arXiv:1910.13970.
99. Yang, W.; Giarè, W.; Pan, S.; Di Valentino, E.; Melchiorri, A.; Silk, J. Revealing the effects of curvature on the cosmological models. *arXiv* **2022**, arXiv:2210.09865.
100. Benisty, D.; Mifsud, J.; Said, J.L.; Staicova, D. On the Robustness of the Constancy of the Supernova Absolute Magnitude: Non-parametric Reconstruction & Bayesian approaches. *arXiv* **2022**, arXiv:2202.04677.
101. Ferramacho, L.D.; Blanchard, A.; Zolnierowski, Y. Constraints on C.D.M. cosmology from galaxy power spectrum, CMB and SNIa evolution. *Astron. Astrophys.* **2009**, *499*, 21. [CrossRef]
102. Linden, S.; Virey, J.M.; Tilquin, A. Cosmological Parameter Extraction and Biases from Type Ia Supernova Magnitude Evolution. *Astron. Astrophys.* **2009**, *50*, 1095–1105. [CrossRef]
103. Tutusaus, I.; Lamine, B.; Dupays, A.; Blanchard, A. Is cosmic acceleration proven by local cosmological probes? *Astron. Astrophys.* **2017**, *602*, A73. [CrossRef]
104. Di Valentino, E.; Gariazzo, S.; Mena, O.; Vagnozzi, S. Soundness of Dark Energy properties. *JCAP* **2020**, *07*, 045. [CrossRef]
105. Perivolaropoulos, L.; Skara, F. A reanalysis of the latest SH0ES data for H_0: Effects of new degrees of freedom on the Hubble tension. *Universe* **2022**, *8*, 502. [CrossRef]
106. de Carvalho, E.; Bernui, A.; Avila, F.; Novaes, C.P.; Nogueira-Cavalcante, J.P. BAO angular scale at zeff = 0.11 with the SDSS blue galaxies. *Astron. Astrophys.* **2021**, *649*, A20. [CrossRef]